Effect of liquid films on the isothermal drying of porous media

A. G. Yiotis,[1,2] A. G. Boudouvis,[1] A. K. Stubos,[2] I. N. Tsimpanogiannis,[3] and Y. C. Yortsos[3,*]
[1]*School of Chemical Engineering, National Technical University of Athens, Zografos 15780, Greece*
[2]*National Center for Scientific Research "Demokritos," Aghia Paraskevi 15310, Greece*
[3]*Department of Chemical Engineering, University of Southern California, Los Angeles, California 90089-1211, USA*
(Received 23 June 2003; published 26 September 2003; published 29 September 2003)

We study the effects of liquid films on the isothermal drying of porous media. They are important for the transport of liquid to an evaporation interface, far from the receding liquid clusters. Through a transformation, the drying problem is mapped to the Laplace equation around the percolation liquid clusters. From its solution, the properties of drying are obtained in terms of the capillary number. Consistent with experimental evidence, film flow is shown to accelerate drying significantly.

DOI: 10.1103/PhysRevE.68.037303 PACS number(s): 47.55.Mh, 47.55.Kf, 64.60.Ak, 64.70.Fx

The drying of porous media is an important process [1], finding applications to areas such as wood, paper, and the textile industry, the drying of foodstuff and pharmaceutical products, and the remediation of contaminated soils by vapor extraction. The problem was originally addressed using phenomenological equations [1]. Recent work has focused on pore-level studies [2], which have improved significantly our understanding of the process. Like many phase-change processes in porous media [3], drying is a drainage process, where the evaporating liquid is effectively displaced by a nonwetting gas. In the absence of viscous effects, the patterns of the receding liquid interfaces are those of invasion percolation (IP) [4], with mass transfer in the gas phase controlling the rates by which the liquid clusters recede. IP applies at low drying rates (which always occur at the later stages of the process). Elaborate pore-network models have been developed to account for viscous effects [5–8], advection and transients in the gas phase [7], and temperature gradients [9].

In all these, films have not been considered. The gas-liquid interface was assumed only in the conventional form of menisci spanning a pore-throat cross section. Such menisci will recede to adjacent pores, when the pressure difference exceeds the pore-throat capillary threshold. In realistic (e.g., polygonal) pore geometries, however, this movement is accompanied by the formation of macroscopic liquid films along the pore surface. The films provide hydraulic conductivity and can be important in the transport of mass. Previous experimental work on drying reported on their existence and speculated on their role [2,5,10].

Laurindo and Prat [2] visualized drying in etched-glass micromodel experiments and compared their results to predictions from a pore-network simulator, which did not include films. A mismatch between experimental and simulation drying rates by a factor of six was reported, and attributed to liquid films. Shaw [10] found that the drying front in a cell containing packed beads receded one order of magnitude faster than when the cell was empty. He also attributed this enhancement to fluid counterflow through films, and argued that film flow is the dominant mechanism in the drying of porous materials. This seemingly important mechanism has not been accounted for or explained in previous models, despite many efforts. The purpose of this paper is to close the gap and provide a theory that accounts for film flow and is consistent with the experimental findings.

Consider the isothermal evaporation of a single-component liquid in a porous medium, one end of which is open to the ambient environment, which is kept fully dry (Fig. 1) (see [8] for nonisothermal effects). All other ends are no-flux boundaries. At any stage, we distinguish three kinds of pores (Fig. 1): pores *L*, fully occupied by liquid, pores *G*, fully occupied by gas, and pores *F*, occupied by gas but also containing macroscopic liquid films. All pores are surrounded by an interconnected solid matrix. The existence of pores of type *F* is a distinct feature of this work. We stress that our focus is on macroscopic (thick) films, e.g., which form in the corners of polygonal pores, and where flow is driven by capillary pressure gradients. Thin films, which have very low flow conductivity (e.g., [11]), are neglected. We will account for viscous effects in the films (*F* pores), but not in the continuous liquid and gas (regions *L* and *G*). Mass transfer in the gas is assumed by diffusion. These assumptions are typically valid in drying problems [2,7] (see also [8]).

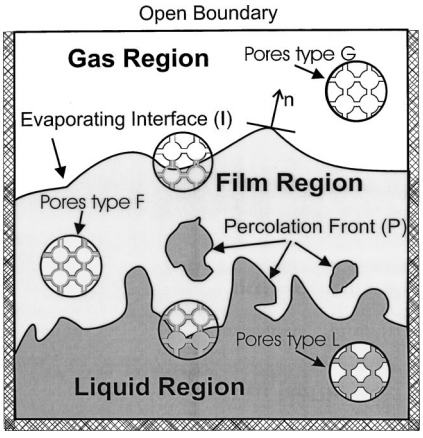

FIG. 1. Schematic of liquid and gas phase patterns in drying, indicating the various types of pores present. The gas phase in the film region *F* is saturated, with evaporation occurring at the film tips (interface I). The boundary of the liquid clusters *P* follows locally IP patterns, and recedes at a rate dictated by film flow through each cluster.

*Corresponding author. Email address: yortsos@usc.edu

 ©2003 The American Physical Society

We will parametrize a film by its radius of curvature $r(\mathbf{x},t)$. Assuming capillary equilibrium the pressure in the film is $P_l = -\gamma/r$, where γ is the surface tension, and where without loss we set the gas pressure, P_g, to zero. Because the films are macroscopic, and the pore geometry fixed, their thickness is proportional to r. Flow in the film is viscous, described by a Poiseuille-type law [12], e.g., $Q_x = -(\alpha r^4/\mu_l)(\partial P_l/\partial x)$, for the volumetric flow rate Q_x along direction x. Here, μ_l is liquid viscosity and α a dimensionless constant, depending on film and throat geometry [12]. For a single liquid film in a throat of a square cross section, and of zero contact angle, $\alpha = 0.0022$.

To proceed, we must write mass balances for the evaporating species in the film and in the gas, and couple them to the liquid and gas regions. Given the complexity of the pore space this is not trivial. However, meaningful progress is possible with a relatively simple approach. For this, we need insight from the physics of a single film in a long capillary, extending along direction x. The mass balance in such a film is

$$\beta \frac{\partial r^2}{\partial t} = \left(\frac{\alpha \gamma}{3\mu_l} \right) \frac{\partial^2 r^3}{\partial x^2} - Q_e, \tag{1}$$

where β is another constant, the evaporation rate is approximately $Q_e \approx \delta D r (C_e - C)/\rho_l R$, D is an effective mass diffusivity, C is the cross-sectionally averaged mass concentration in the gas, with C_e the equilibrium value, ρ_l is liquid density, and R is an equivalent throat size. For a square capillary, $\beta \approx [1-(\pi/4)]$ and $\delta \approx \pi/2$. Correspondingly, the mass balance in the gas is

$$\frac{\partial C}{\partial t} = D \frac{\partial^2 C}{\partial x^2} + \frac{m \rho_l Q_e}{A_p}, \tag{2}$$

where $A_p \sim R^2$ is the capillary area and m the number of films in the capillary. We must emphasize that Eqs. (1) and (2) capture only integral characteristics of the film. Absent are many detailed, locally important phenomena, such as Marangoni instabilities, van der Waals attraction, and nonisothermal evaporation [13]. However, as noted above, and further illustrated below, our objective is to capture leading-order effects of isothermal drying at the pore-network scale, which extends over a multitude of pores. We submit that these are adequately represented with the simpler description in Eqs. (1) and (2).

The two equations (1) and (2) were solved elsewhere [8]. Two key results were found: (i) A steady state in the r and C profiles is rapidly established, and (ii) for practical purposes, evaporation occurs only near the film tip, in a region extending over a few capillary radii. The development of a steady state is expected and it is common to other diffusion-type processes in disordered media [15]. The fact that evaporation is restricted to a narrow region is a consequence of the confined narrow geometry of the capillary. The gas phase becomes rapidly saturated and the concentration decays exponentially, hence evaporation is limited to the region near the film tips. Capillarity-driven film flow supplies the required liquid flux.

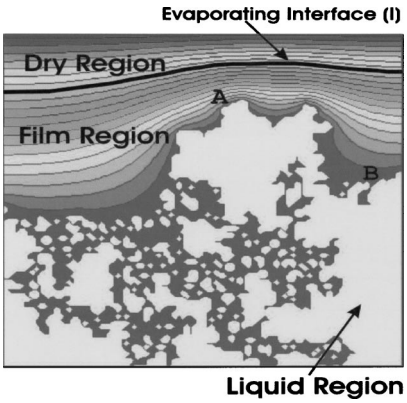

FIG. 2. Isocontours of the solution of the Laplace equation around the clusters of the drying front, with boundary conditions $\Phi = 1$ at the front and $\Phi = 0$ at the open end.

It is not difficult to accept that the same physics also apply to a network of capillaries (pores). Therefore, we submit that the drying of porous media can be simplified using the same two approximations. Thus (i) in region F, the gas phase is saturated ($C = C_e$), evaporation does not occur, and the film flow is steady. By using the dimensionless variables $\zeta \equiv C/C_e$ and $\rho \equiv r/r_0$, where r_0 is a characteristic film radius (or a roughness scale [14]), we then have

$$\nabla^2 \rho^3 = 0 \quad \text{and} \quad \zeta = 1 \quad \text{in region} \quad F. \tag{3}$$

In Eq. (3) we used the Laplace equation as the analog of the steady state of Eq. (1). We also assumed locally constant geometries (hence transport coefficients) and have upscaled the problem, such that now r (or ρ) stands for an appropriately volume-averaged radius. A similar approach was used for Eq. (4). (ii) In region G, films are absent and mass transfer is by steady-state diffusion, thus

$$\nabla^2 \zeta = 0 \quad \text{and} \quad \rho = 0 \quad \text{in region} \quad G. \tag{4}$$

(iii) Finally, evaporation is assumed to occur across the evaporation interface I (Figs. 1 and 2), where $r = 0$ and $C = C_e$. Then, a mass balance leads to the following dimensionless equation:

$$\frac{1}{\mathrm{Ca}} \frac{\partial \rho^3}{\partial n} = \frac{\partial \zeta}{\partial n} \quad \text{at interface} \quad I \quad \text{where} \quad \rho = 0 \quad \text{and} \quad \zeta = 1 \tag{5}$$

and where n is the unit normal to the interface. Equations (3)–(5) describe the problem in the regions outside the liquid clusters. They depend on only a one-dimensionless parameter, the effective capillary number $\mathrm{Ca} \equiv 3\mu_l A_p D C_e / m \alpha \gamma r_0^3 \rho_l$. Drying is driven by the conditions $\zeta = 0$ at the open end of the domain and $\rho = 1$ at the cluster perimeter (Fig. 1). An initially wet porous medium is considered.

Given that the location of interface I is unknown, the problem appears rather complex. Closer inspection, however, reveals that a simple transformation can lead to a straightforward solution. For this, note that ρ and ζ satisfy the same Laplace equation in their respective, mutually exclusive, do-

mains F and G (where ζ and ρ are, respectively, constant). Further, at the dividing interface I, the normal fluxes of ρ and ζ are linearly related [through Eq. (5)]. Thus, the linear combination

$$\Phi \equiv \frac{\rho^3 + \zeta \mathrm{Ca}}{1 + \mathrm{Ca}} \tag{6}$$

satisfies the Laplace equation *everywhere* (in regions F and G), including interface I, where Φ is continuous and has continuous derivatives. Thus, finding the ρ and ζ profiles requires solving the Laplace equation for Φ in the domain $F+G$, subject to the conditions $\Phi=1$ at the liquid cluster interface P, and $\Phi=0$ at the open end. Interface I, where the films terminate, is located simply as the position where $\Phi = \mathrm{Ca}/(\mathrm{Ca}+1)$.

To solve the complete problem requires knowledge of the location of interface(s) P. However, assuming that viscous effects are negligible in the bulk liquid clusters, their interface is recursively obtained using IP rules, namely by invading at every receding step the pore throat with the largest radius (e.g., see [2] and schematics of Figs. 1 and 2). This process, as is known by previous studies [4] is described by the well-studied IP. In addition, during drying, liquid clusters of finite size become disconnected and macroscopically isolated (Figs. 1 and 2, see also [7]). However, films emanating from such clusters are automatically included in the above description, the rates by which a given cluster drains being dictated by the total flow rate through these films.

For a numerical illustration, we solved the problem in a square lattice of size 150×150. The lattice is assumed to represent the pore network. Other lattice types (e.g., cubic, hexagonal, etc.) are of course possible. The equation for Φ was solved for successive positions of the receding liquid-gas interface P, using finite-differences and a successive-overrelaxation (SOR) scheme. The interface P was determined recursively using IP algorithms (e.g., see [2,7]). Figure 2 shows a snapshot of the iso-potential contours. They reflect the solution of the Laplace equation around the various percolation clusters, and display fractal features at close distances, becoming smoother at a distance away. Figure 2 depicts numerically the schematics of Fig. 1. Percolation patterns of the type shown in Fig. 2 were reported in both the experiments of Shaw [10] and Laurindo and Prat [2]. Figure 2 also shows the location of the film tips (evaporation interface I) for the specific value of $\mathrm{Ca}=0.1$ (where $\Phi=1/11$). Figure 3 shows the profile of the normalized film radius ρ, corresponding to the same drying stage, but with two different Ca values, $\mathrm{Ca}=10^{-4}$ and $\mathrm{Ca}=1$, respectively. At low Ca [Fig. 3(a)], the films are shown to extend all the way to the open end, which is the place where all evaporation practically occurs. However, when Ca is $O(1)$, the films are shorter [Fig. 3(b)], leading to the formation of a completely dry region G, the extent of which increases with time.

Based on Eq. (6), the overall drying rate $\mathcal{F}$ for a two-dimensional (2D) geometry can be shown to scale as

$$\mathcal{F} = -\frac{\phi D l C_e (1+\mathrm{Ca})}{\mathrm{Ca}} \mathcal{F}_{\mathcal{D}} \quad \text{where} \quad \mathcal{F}_{\mathcal{D}} \equiv -\int_{a_0} \frac{\partial \Phi}{\partial n} da. \tag{7}$$

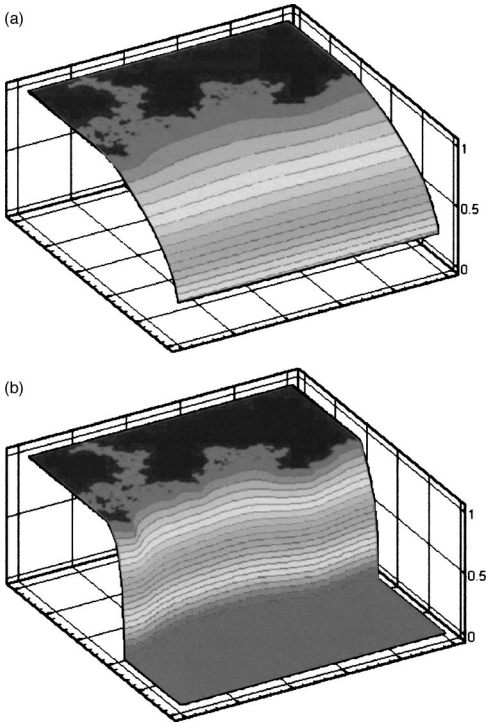

FIG. 3. Dimensionless film thickness profiles (ρ vs the lattice coordinates) for two different values of Ca [equal to 10^{-4} and 1, in (a) and (b), respectively], corresponding to the same extent of drying.

Here, ϕ is porosity (assumed constant), l is a typical pore length, and subscript 0 denotes the open boundary. $\mathcal{F}_{\mathcal{D}}$ is only geometry (and time) dependent. For convenience, we parametrize time by the characteristic time to drain a pore of volume V_p from its liquid, namely,

$$t^* = \frac{V_p \rho_l \mathrm{Ca}}{\phi D C_e l (1+\mathrm{Ca})}. \tag{8}$$

In this notation, the dimensionless time interval $\Delta\tau$ to advance a pore is $\Delta\tau = -1/\int_{a_0}(\partial\Phi/\partial n)da$, from which the dimensionless time τ can be obtained by integration.

Figure 4 shows a log-log plot of the gas saturation S_g, defined as the fraction of the total liquid evaporated compared to the initial vs the dimensionless time τ. This curve is the ensemble average of ten Monte Carlo realizations. It depends *only on the geometry of the pore space* and it is the same for *any* value of Ca (therefore, also for the case of no films, e.g., as in [2]), as noted above. The dependence on Ca enters upon converting Fig. 4 to dimensional time. As Eq. (8) shows, this is obtained by shifting the $\log\tau$ axis by $\log t^*$ (which at $\mathrm{Ca}\ll1$ is equal to shifting $\log \mathrm{Ca}$). It follows that an order of magnitude decrease in Ca leads to an order of magnitude decrease in time and a corresponding increase in the drying rate.

We summarize our findings as follows: The extent of the wetting films in drying increases with $(\mathrm{Ca}+1)/\mathrm{Ca}$, namely, with smaller values of Ca. The latter is favored by larger interfacial tension, larger r_0, and smaller viscosity and effective diffusivity. The latter is a lumped parameter in our

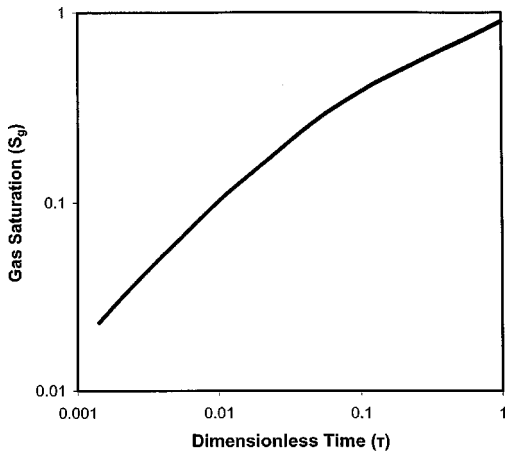

FIG. 4. Plot of the gas saturation S_g vs the dimensionless time τ. This curve depends solely on the geometry of the medium and the pore space.

model and may be different than the molecular diffusivity, to reflect additional mechanisms at the film tip [13] which were neglected here. The drying rate increases as Ca decreases [by the factor $\phi DlC_e(1+\mathrm{Ca})/\mathrm{Ca}$], which at small Ca is inversely proportional to Ca and scales as $\sim \phi l \gamma r_0^3/\mu_l A_p$. We reiterate that this is not an issue of increased film surface area, given that evaporation is practically restricted to the film tips. Rather, at smaller Ca, capillarity helps to transport liquid over larger distances, thus leading to steeper concentration gradients, as the film tips (and interface *I*) are closer to the open boundary, and hence to larger evaporation rates. Conversely, at larger Ca, the film extent is smaller, films do not contribute substantially, and the drying rates decrease. All previous pore-network models [2,6,7] correspond effectively to such condition of large Ca. In typical problems, where the capillary numbers is generally much less than $O(1)$, we anticipate the existence of long films that drain, through the above ''wicking'' action, liquid all the way to the open end, where it subsequently evaporates. For instance, in the experiments in [2] we have the rough estimate Ca $\sim 10^{-4}$, suggesting that liquid films (region *F*) likely existed in all gas-invaded pores and that a completely dry region (region *G*) did not develop.

We close by briefly commenting on the conjecture by Shaw [10] regarding the scaling of the front width (namely, of the interface *P* in Figs. 1 and 2) and the interpretation in [5]. In the absence of films, a point of the interface closer to the open end (e.g., at point *A* compared to *B*, Fig. 2) would have larger evaporation rates, due to the compression of the concentration contours. This would lead to increased liquid flow rates towards point *A* (e.g., from point *B* to point *A*), and to a concomitant gradient in the percolation probability. The same argument also applies in the presence of films: Films emanating from point *A* will be closer to the open end, hence they would carry a higher liquid flow rate (e.g., compared to films from point *B*), due to the increased evaporation at their tip. This higher rate would require increased flow within the liquid cluster towards point *A*, leading to the same conclusions as in the above argument in the absence of films.

In this paper we studied the effect of wetting liquid films in the isothermal drying of porous materials. Generally considered a daunting task, this effect was accounted for by using a unique transformation. Simple scaling relations show that the drying rate increases as Ca decreases, but it saturates to a constant at high values of Ca. The results show that film flow can be an important mechanism for drying, consistent with available experimental evidence.

This work was partly supported by DOE Contract DE-AC26-99BC15211, the contribution of which is gratefully acknowledged.

[1] S. Whitaker, Adv. Heat Transfer **31**, 1 (1998).
[2] M. Prat, Int. J. Multiphase Flow **21**, 875 (1995); J. B. Laurindo and M. Prat, Chem. Eng. Sci. **51**, 5171 (1996).
[3] Y. C. Yortsos and A. K. Stubos, Curr. Opin. Colloid Interface Sci. **6**, 208 (2001).
[4] D. Wilikinson and J. F. Willemsen, J. Phys. A **16**, 3365 (1983); R. Lenormand and C. Zarcone, Phys. Rev. Lett. **54**, 2226 (1985); D. Wilkinson, Phys. Rev. A **34**, 1380 (1986).
[5] I. N. Tsimpanogiannis *et al.*, Phys. Rev. E **59**, 4353 (1999).
[6] M. Prat and F. Bouleux, Phys. Rev. E **60**, 5647 (1999).
[7] A. G. Yiotis *et al.*, Adv. Water Resour. **24**, 439 (2001).
[8] A. G. Yiotis *et al.* (unpublished).
[9] F. Plourde and M. Prat, Int. J. Heat Mass Transfer **46**, 1293 (2003).
[10] T. M. Shaw, Phys. Rev. Lett. **59**, 1671 (1987); J. B. Laurindo and M. Prat, Chem. Eng. Sci. **53**, 2257 (1998).
[11] P. G. de Gennes, in *Physics of Disordered Materials*, edited by D. Adler, H. Fritzche, and S. R. Ovskinsky (Plenum Press, New York, 1985), p. 227.
[12] T. C. Ransohoff and C. J. Radke, J. Colloid Interface Sci. **121**, 392 (1988); M. Dong and I. Chatzis, *ibid.* **172**, 278 (1995); D. Zhou, M. Blunt, and F. M. Orr, Jr., *ibid.* **187**, 11 (1997).
[13] A. M. Cazabat *et al.*, Nature (London) **346**, 824 (1990); J. A. Schonberg, S. DasGupta, and P. C. Wayner, Jr., Exp. Therm. Fluid Sci. **10**, 163 (1995); D. E. Kataoka and S. M. Troian, J. Colloid Interface Sci. **192**, 350 (1997); A. Oron, S. H. Davis, and S. G. Bankoff, Rev. Mod. Phys. **69**, 931 (1997).
[14] R. Lenormand and C. Zarcone (unpublished); A. L. Dullien *et al.*, J. Colloid Interface Sci. **127**, 362 (1997); G. N. Constantinides and A. C. Payatakes, Transp. Porous Media **38**, 291 (2000).
[15] T. A. Witten and L. M. Sander, Phys. Rev. Lett. **47**, 1400 (1981); *The Science of Fractal Images*, edited by H-O. Peitgen and D. Saupe (Springer-Verlag, Berlin, 1988); C. Satik and Y. C. Yortsos, Trans. ASME, Ser. C: J. Heat Transfer **118**, 455 (1996).